Available online at **www.joac.info**

ISSN: 2278-1862

Journal of Applicable Chemistry

2020, 9 (5): 774-788

(International Peer Reviewed Journal)

Electrochemical and Quantum Chemical Studies of 1-(4-Nitrothiophen-2-Yl)-3-(4-(Prop-2-Yn-1-Yloxy) Phenyl) Prop-2-En-1-One on the Corrosion Inhibition of 6063 Al in Hydrochloric Acid

K. Aparna[1], Balakrishna Kalluraya[1]* and K. Raviprabha[2]

1. Department of Chemistry, Mangalore University, Mangalagangothri-574199, **INDIA**
2. Department of Chemistry, Shri MadwaVadiraja Institute of Technology, Bantakal-574115,Karnataka, **INDIA**

Email: bkalluraya@gmail.com

Accepted on 9th August, 2020

ABSTRACT

A new chalcone 1-(4-nitrothiophen-2-yl)-3-(4-((prop-2-yn-1-yl)oxy)phenyl)prop-2-en-1-one(NPOP) was synthesized by the condensation of 4-nitro acetyl thiophene and propargylated benzaldehyde and was characterized by IR, ^{1}H NMR and Mass spectra. Corrosion inhibition property of NPOP on 6063 Al alloy in 0.5M HCl were studied using weight loss, potentiodynamic polarization and electro-chemical impedance spectroscopy (EIS) method. The inhibition efficiency was raised with increase in concentration of the inhibitor and temperature. The chalcone acted as a mixed type of inhibitor and its adsorption on mild steel surface was found to follow Langmuir's adsorption isotherm. Thermodynamic adsorption functions and the activation parameters were also calculated and analysed. All the studied parameters showed excellent inhibitory properties of NPOP against corrosion of alloy in 0.5M HCl.

Graphical Abstract

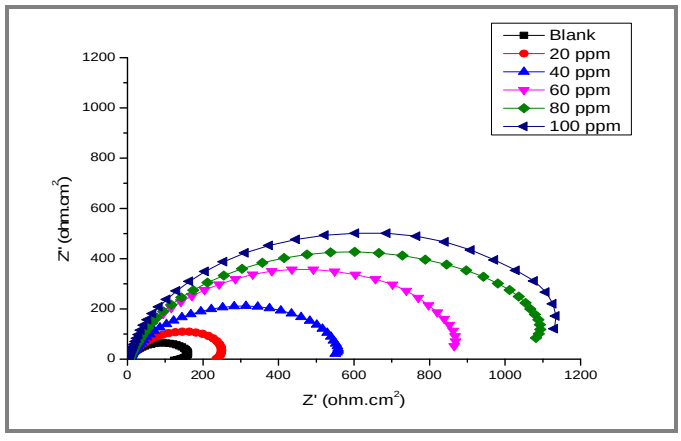

Nyquist plot for corrosion of 6063Al alloy in 0.5M HCl with various concentrations of NPOP at 333K.

Keywords: Corrosion, 6063Al alloy, HCl, SEM, Quantum chemical studies.

INTRODUCTION

Aluminium which has a small atomic mass and negative value with the standard reduction potential may attract as an anodic material to energy sources with elevated energy density [1]. Due to relative excellent resilience to corrosion, formability and low price, 6063 Al alloys are widely used in the aerospace, house hold, electric, automotive, marine and other construction sectors [2]. The most important feature of aluminium is its corrosion resistance due to the existence of a thin adherent and protective surface oxide film. However, aluminium and its alloys are reactive and susceptible to corrosion [3].

The enhanced aerosols however deplete the adherent aluminium oxide film and accelerate the corrosion attack in the presence of more severe settings [4, 5]. Even though multiple methods, material choice, anodic and cathodic protection, and several kinds of coating techniques for corrosion control are accessible, it is a time-tested and technically suggested the usage of organic heterocyclic compounds as inhibitors [6, 7]. A number of literatures revealed that most of the inhibitors used for preventing corrosion are organic compounds having oxygen, sulphur, nitrogen and phosphorous in their structure or aromatic rings [8].

Chalcones and their derivatives showed a wide range of pharmacological activities [9-13]. Recently few chalcone derivatives are reported as effective corrosion inhibitors for mild/carbon steel and aluminium in acidic condition [14, 15]. So our primary objective of the current research is to explore the adsorption process and corrosion-inhibition effectiveness of NPOP on the corrosion of 6063Al alloy in 0.5M HCl media. The research also examines the detailed mechanism of inhibition by taking into account adsorption isotherms as well as kinetic and activation parameters.

MATERIALS AND METHODS

Synthesis of NPOP: A solution of substituted aldehyde (0.1 mol) and corresponding acetophenone (0.1 mol) in glacial acetic acid (25 mL) was treated with conc. H_2SO_4 (1-2 mL). The mixture was stirred at room temperature for 24 h. Precipitated product of propenones were collected by filtration, washed with water and recrystallized from suitable ethanol [12] (Figure 1). The compound was characterized by IR and NMR spectroscopic method. Pale yellow solid; Yield: 80%, m.p.: 170-172°C; IR (KBr,cm^{-1}):3107(Ar-H) , 3224(≡C-H), 1570 (C=C), 1643(C=O), 2100 (C≡C), 1504 and 1336(NO_2 symmetric and asym.); ^{1}H NMR(400MHz,$CDCl_3$) δ:3.38(t,1H,J=2.8Hz,alkyne CH),4.7(d, 2H, J=2.28Hz, OCH_2), 7.13(d, 2H, J=8Hz,Ar-H),7.35(s, 1H ,J=4Hz, thiophene-H), 7.56 (s,1H J=15.56Hz, α-CH), 7.69(s, 1H, J= 4Hz, thiophene-H), 7.86(s, 1H, J=15.56, 56Hz,β-CH), 8.11(d, 2H, J=8Hz, Ar-H); MS:m/z =314.00 (M^++1).

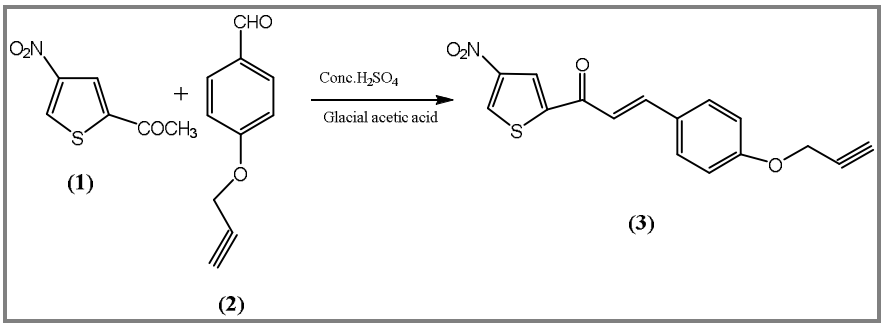

Figure 1. scheme for the synthesis of NPOP

Corrosive and inhibitory medium: 37% HCl was diluted to prepare 0.5M Hydrochloric acid (HCl) solution using double distilled water. Normalization of HCl was performed by volumetric technique

using NaOH solution. Various other solutions are prepared from the stock solution of HCl(0.5M). Inhibitor used in the present study is 1-(4-nitrothiophen-2-yl)-3-(4-(prop-2-yn-1-yloxy)phenyl)prop-2-en-1-one(NPOP). The inhibition effect was investigated in a 20-100 ppm of NPOP solution using calibrated thermostat at temperatures between 303K, 313K, 323K, and 333K under unstirred and ventilated conditions.

Preparation of test coupons: 6063Al alloy specimen was purchased from PMC, Bangalore. The basic composition of 6063 Al alloy (%w) was: Si-0.41, Fe-0.11, Cu-0.05, Mg-0.49, Cr-0.1, Mn-0.1, Ti-0.1 and remainder-Al. The Aluminium specimen was taken in the form of a cylindrical rod with 1.31cm^2 exposed surface areas, remaining was entrenched in epoxy resin. According to metallographic practice, the specimen was polished using various grades of emery paper and mirror finish was obtained on disc polishing using legated alumina. Double distilled water followed by acetone was used to clean the specimen, finally dried and immediately used for the analysis.

Weight loss method: The 6063 Al alloy coupons of dimensions 1.5 cm ×2.5 cm×1 cm were used for the measurement of weight loss. They were polished with various grades of emery paper and then washed with distilled water and acetone. The coupons were immersed for about 4, 8 and 12 h in 0.5 M HCl solutions comprising different inhibitor levels at 303K. Coupons were subsequently removed from the test solutions, cleaned with anhydrous alcohol, dried and then weighed.

Equations 1 and 2 were used to calculate inhibition effectiveness and corrosion rate.

$$IE(\%) = \frac{W_0 - W_{in}}{W_0} \times 100 \qquad (1)$$

$$CR(mm/year) = 87.6 \times (\Delta W / Atd) \qquad (2)$$

In the equation A refers area of the specimen , d is density, of Al in gcm^{-3}, T is time in hours; W_0 is weight loss without NPOP and W_{in} weight loss with NPOP.

Electrochemical studies: Potentiostat (CH604 E-series, U.S. model with CH-instrument beta software) was used to perform electrochemical readings of 6063Al alloy. Both polarization experiments and electrochemical impedance measurements (EIS) are performed using standard three-electrode glass cell with Platinum counter electrode and saturated calomel electrode as reference and 6063Al alloy specimen as working electrode. In the presence and absence of NPOP at different temperatures, the freshly polished specimen was exposed to a corrosive medium of 0.5 M HCl and permitted the establishment of a steady state open circuit potential. The EIS studies were performed by impressing open-circuit potential of 10 mV amplitude AC signal with a frequency range from 10000 Hz to 0.01 Hz. Nyquist plots were used for the analysis of impedance data to assess corrosion characteristics.

Surface morphology studies: Surface Morphology Study of 6063Al Alloy was conducted in 1000X magnification using an analytical electron scanning microscope (JEOL JSM-6380L). A metal sample surface morphology was acquired by immersing the sample in hydrochloric acid medium for 2 h in absence and in presence of inhibitor.

Quantum chemical study: In order to detect the correlation of the molecular structure and the inhibition effectiveness, Quantum chemical calculations based on DFT/B3LYP level were performed using Gaussian 03 software for windows. The molecular structure of NPOP was fully and geometrically optimized using Becke's three-parameter, Lee–Yang–Parr exchange correlation function in conjugation with 6-31G (d,p) basis set.

RESULTS AND DISCUSSION

Weight loss analysis: Table 1 listed the weight loss data for the 6063 Al alloy corrosion phenomenon in 0.5 M HCl at 303K.The protective effectiveness of NPOP is noted as being improved linearly in the corrosive medium with its greater concentration range. At 100 ppm of NPOP showed the highest inhibition efficiency of 89.5%. Nearly the same effectiveness was achieved above this concentration; therefore, it is regarded to be the optimum concentration for attaining maximum inhibition effectiveness. The variation of weight loss and inhibition efficiency at varying immersion times is given in figure 2 and 3.

Table 1. Weight loss results of various concentrations of NPOP at different immersion time.

Immersion Time (Hours)	Conc. Of inhibitor	Wt. loss (mg)	C.R (mm years^{-1})	%IE
4	Blank	2.50	17.95	--
	20 ppm	0.71	5.02	72.0
	40 ppm	0.65	4.66	74.0
	60 ppm	0.53	3.80	78.8
	80 ppm	0.44	3.16	82.4
	100 ppm	0.39	2.8	84.4
8	Blank	6.44	23.11	--
	20 ppm	1.55	5.56	75.9
	40 ppm	1.31	4.70	79.7
	60 ppm	1.11	3.98	82.8
	80 ppm	0.98	3.51	84.8
	100 ppm	0.85	3.05	86.8
12	Blank	14.30	34.17	--
	20 ppm	3.12	7.46	78.2
	40 ppm	2.80	6.69	80.4
	60 ppm	2.21	5.26	84.6
	80 ppm	1.85	4.42	87.1
	100 ppm	1.50	3.59	89.5

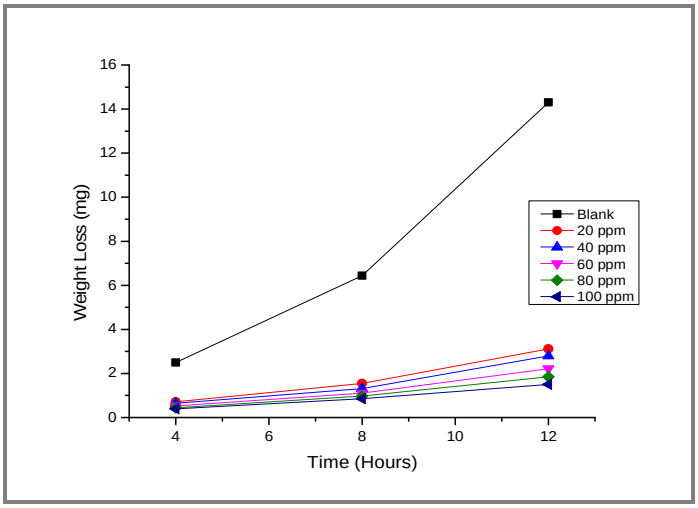

Figure 2. Weight loss of 6063 Al alloy in 0.5M HCl solution with and without the addition of NPOP at 303K with different immersion time.

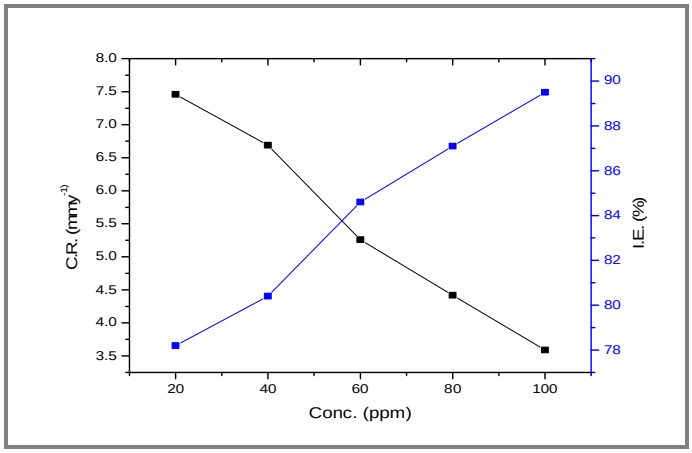

Figure 3. Variation of the inhibition efficiency and corrosion rate with concentration of NPOP in 0.5M HCl.

Potentiodynamic polarization (PDP) study: The impact of inhibitor concentration on 6063Al alloy corrosion rate was investigated and represented by figure 4.

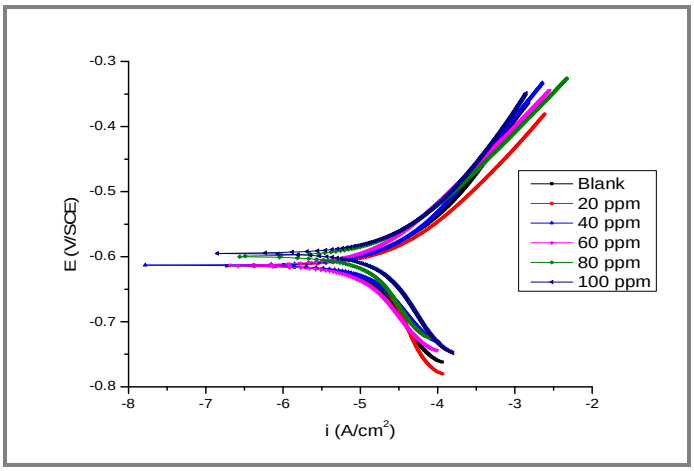

Figure 4. Potentiodynamic polarisation plots for 6063Al alloy in 0.5M HCl with various concentrations of NPOP at 333K.

The electrochemical components such as the corrosion current (i_{corr}), corrosion potential (E_{corr}) were acquired from PDP measurement. The corrosion rate (C.R.) is calculated using the Equation (3).

$$C.R. = \frac{3270 \text{ X M X icorr}}{\rho \; X \; Z} \qquad (3)$$

3270 defines unit of corrosion rate, ρ is the density of Aluminium, M is the atomic mass, Z is the number of electrons [**16**]. Equation (4) is used to calculate the inhibition efficiency.

$$\eta = \frac{i_{corr(un)} - i_{corr(in)}}{i_{corr(un)}} \times 100 \qquad (4)$$

Where $i_{corr(un)}$ is the corrosion current in the absence and $i_{corr(in)}$ corrosion current in the presence of the inhibitor. Table 2 lists the results of the measurement of potentiodynamic polarization (Tafel

polarization) for corrosion of 6063 Al alloy at 0.5 M HCl comprising distinct inhibitor levels at distinct temperatures. It obviously demonstrates that in the presence of distinct inhibitor levels, the corrosion current (i_{corr}) and corrosion rate (C.R.) values reduce. Therefore, the effectiveness of inhibition improves with a rise in the inhibitor of concentration. The highest corrosion rate was found at higher temperatures, i.e. 333K, in the blank sample shown in table 3, but the highest inhibition effectiveness was at 333 K (89.4%). This is primarily due to the adsorption inhibitor.

Table 2. Results of Tafel polarisation studies on 6063Al alloy in 0.5M HCl solution containing various concentrations of inhibitor

Temp (K)	Concentration (ppm)	-Ecorr (mV)	βc (mV)	βa (mV)	Icorr (mA/cm^2)	CR (mmpy)	IE(%)
303	Blank	630	59.7	197.3	7.36	20.84	-
	20	628	57.2	191.9	1.95	5.33	73.51
	40	628	55.4	187.6	1.65	5.25	77.58
	60	623	56.4	159.5	1.42	5.15	80.71
	80	619	52.9	140.6	1.26	4.46	82.88
	100	618	50.4	134.1	1.09	4.11	85.19
313	Blank	625	62.7	185.8	12.44	39.92	-
	20	624	66.8	180.6	2.95	7.31	76.29
	40	621	64.3	177.5	2.52	6.91	79.74
	60	621	62.8	148.4	2.31	6.37	81.43
	80	623	63.1	142.3	2.06	5.85	83.44
	100	617	58.7	136.7	1.65	5.36	86.74
323	Blank	619	72.4	124.4	12.44	78.69	-
	20	620	70.1	121.6	3.58	10.13	77.97
	40	618	69.9	114.9	3.11	9.97	80.86
	60	618	68.8	113.5	2.95	8.87	81.85
	80	617	56.9	108.7	2.56	7.55	84.25
	100	615	56.6	108.2	2.05	6.13	87.38
333	Blank	614	77.3	121.0	20.56	92.61	-
	20	613	70.3	129.5	4.25	12.65	79.32
	40	613	66.6	117.1	3.80	11.40	81.51
	60	614	62.5	109.0	3.20	9.21	84.43
	80	600	55.9	125.9	2.63	8.05	87.21
	100	595	54.9	101.9	2.11	6.95	89.74

It is reported in literature [**17, 18**] that, the inhibitor may be considered distinctively as an anodic and cathodic inhibitor when the corrosion potential (Ecorr) value of the inhibited solution is less than ±85 mV in terms of an uninhibited solution. The peak displacement in the present study, however, significantly below ±85mV. This implies that NPOP may act as a blended inhibitor, with an anodic inhibition predominantly [**19**].

Electrochemical impedance spectroscopy (EIS) measurements: Nyquist plots for the corrosion inhibition of 6063Al alloy in 0.5M HCl medium at various concentration of NPOP at 333K as shown in figure 5. Because of the frequency dispersion of interfacial impedance, owing to roughness and non-homogeneous surfaces, adsorption of the inhibitor and formation of porous layer, Nyquist plots were deviated by semicircles. The impedance spectrum showed that corrosion was regulated primarily through charge transfer process. In figure 5, the high frequency region (HF) corresponds to large capacitive loop while low frequency region (LF) indicates small inductive loop. The large capacitive loop at HF region represents the charge transfer during corrosion process and development of oxide layer on the metal surface [**20**]. The origin of the inductive loop has been attributed to surface or bulk relaxation of species in the oxide layer [**21**]. The LF inductive loop may be related to the relaxation process obtained by adsorption and incorporation of chloride ions, oxide ions or charged species on the electrode surface [**22**]. The Nyquist plot acquired for the corrosion control of 6063 Al indicates that, with rise in the inhibitor concentration, diameter of the capacitive loop increased, owing to a reduction in the rate of corrosion caused by the inhibitor molecule adsorption into the surface of the metal.

Impedance parameters are analysed by fitting a suitable equivalent circuit to the Nyquist plots using $Z_{SimpWin}$ software version 3.21. Figure 6 shows the equivalent circuit, which was used to simulate the impedance plot for 6063Al alloy. The equivalent circuit consists of nine elements. They are solution resistance (R_s) and charge transfer resistance (R_{ct}), inductive resistance (R_L) and the inductive element (L). The CPE (constant phase element, (Q)is parallel to the series of capacitors C_1 and C_2 and also parallel to the series of resistor R_1, R_2, R_L and R_{ct}. R_L is parallel to L inductor. The parallel circuit of a resistor is ascribed, due to ionic conductivity in the oxide film and the capacitance due to its dielectric properties. The double layer capacitance (C_{dl}) and polarization resistance (R_p) can be determined by using the equations,

$$Rp = R_1 + R_2 + R_L + R_{ct} \quad (5)$$

$$Cdl = C_1 + C_2 \quad (6)$$

Equation 7 is used to determine, constant phase element impedance

$$Z = A^{-1}(iw)^{-n} \quad (7)$$

In the above equation proportionality constant is A, w is the angular frequency, i is imaginary number and n is phase shift exponent. If the value of n=1, the CPE will act as an ideal capacitor. The correlation between capacitance and its actual value is calculated using the equation 8 [**23**].

$$Cdl = \frac{1}{2\pi f_{max} Rct} \quad (8)$$

Where f_{max} highest frequency of the imaginary component of impedance and Rct is is resistance to the charge transfer. Cdl values measured were reduced with rise in concentrations of the inhibitor at all temperatures. The reduction in Cdl value was caused by increase in electrical double layer at the metal solution interface. The slow replacement of inhibitor molecules with water molecules causes further decrease of Cdl values. The polarization resistance (R_P) values vary inversely with corrosion current density (icorr). Equation 9 was used to get the inhibition efficiency.

$$IE(\%) = \frac{R_p\ inh - R_p}{R_p(inh)} \times 100 \quad (9)$$

R_P values improved with enhanced inhibitor concentration. This leads to a reduction in the value of double layer capacitance (Cdl), indicating that the method of transfer of charge primarily controls the process of corrosion.

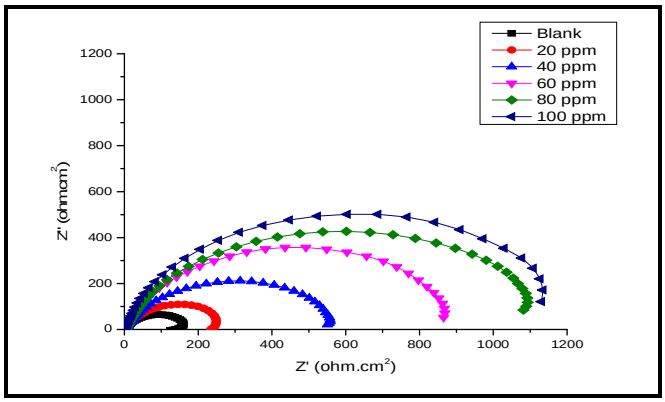

Figure 5. Nyquist plot for corrosion of 6063Al alloy in 0.5M HCl with various concentrations of NPOP at 333K.

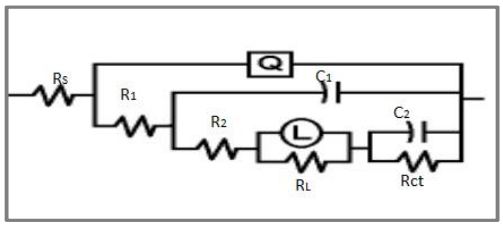

Figure 6. Equivalent circuit used to fit experimental EIS data for the corrosion of 6063Al alloy in 0.5M HCl in the absence and presence of NPOP.

Table 3. Electrochemical impedance values of 6063Al alloy in 0.5M HCl solution containing different concentrations of NPOP at different temperatures

Temp (K)	Concentration (ppm)	Rct (Ωcm^2)	Cdl (µF)	IE (%)
303	Blank	147	401.6	-
	20	464	85.3	68.32
	40	578	63.1	74.57
	60	781	48.9	81.18
	80	897	30.3	83.61
	100	974	25.5	84.91
313	Blank	125	513.0	-
	20	415	91.2	69.88
	40	616	75.6	79.71
	60	725	55.4	82.76
	80	854	48.4	85.36
	100	957	41.0	86.94
323	Blank	110	615.1	-
	20	368	102.3	70.11
	40	595	88.9	81.51
	60	625	63.4	82.40
	80	795	50.0	86.16
	100	980	46.5	88.78
333	Blank	98	819.3	-
	20	340	123.1	71.18
	40	575	99.4	82.96
	60	825	74.3	88.12
	80	1000	54.0	90.20
	100	1100	47.8	91.09

Temperature Effect-Adsorption isotherms: The impact of temperature and inhibition effectiveness of NPOP on the corrosion rate of 6063 Al alloy in 0.05M HCl is investigated at a range of temperatures 303-333K from where kinetic and thermodynamic corrosion inhibition parameters have been computed. The adsorption mechanism can be interpreted by activation energy (Ea) in presence and in absence of inhibitor.

The activation energy is determined by Arrhenius equation 10[24].

$$\ln(C.R.) = A - \frac{Ea}{RT} \qquad (10)$$

Where A is Arrhenius constant, R is gas constant and T is temperature. A straight line in obtained for the plot of ln (C.R.) against 1/T which is shown in figure 7. From the slope of the straight line Ea/R is recorded. Activation energy (Ea) values were calculated for both corrosion and inhibition process.

The enthalpy and entropy of activation is determined using transition state equation 11in the metal dissolution process.

$$CR = \frac{RT}{Nh}\exp\left(\frac{\Delta S \neq}{R}\right)\exp\left(\frac{-\Delta H \neq}{RT}\right) \qquad (11)$$

Where *h* is Plank's constant and N is Avogadro's number.

Figure 8 indicates the plot of ln(CR/T) versus 1/T showing a straight line. The slope of the straight line is $\Delta H^{\neq}/R$ and intercept is $ln\ \frac{RT}{Nh}\exp(\frac{\Delta S\neq}{R})$. Table 4 shows the calculated values for the activation parameters.

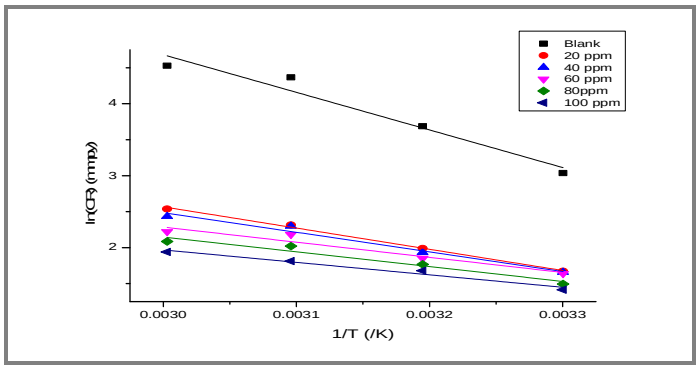

Figure 7. Arrhenius plots for the corrosion inhibition of 6063 Al alloy in 0.5M HCl containing different concentrations of NPOP.

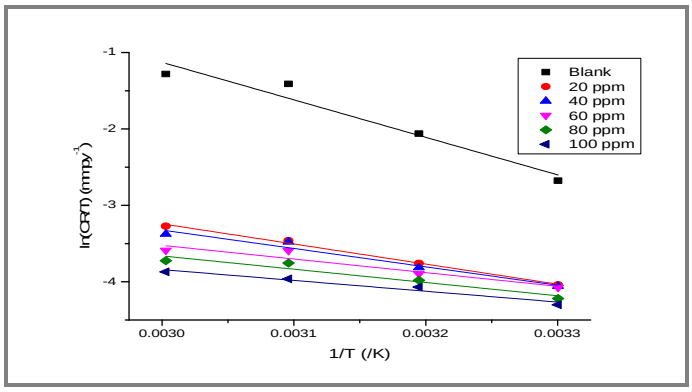

Figure 8. Plots of ln(CR/T) vs. 1/T for the corrosion inhibition of 6063Al alloy in 0.5M HCl containing different concentrations of NPOP.

Table 4. Activation parameters for the corrosion of 6063 Al alloy in 0.5M HCl containing different concentrations of NPOP

Inhibitor concentration(ppm)	Ea ($kJmol^{-1}$)	ΔH ($kJmol^{-1}$)	-ΔS ($Jmol^{-1}K^{-1}$)
Blank	43.46	40.81	101.6
20	24.51	21.88	191.0
40	22.64	20.00	198.6
60	17.48	14.84	219.2
80	17.09	14.45	222.0
100	14.40	11.77	233.5

Energy of activation (Ea) is reduced owing to gradual adsorption of inhibitor molecules on 6063Al alloy, with a rise in inhibitor concentration, but this reduction of Ea value is indicative of the chemical adsorption of inhibitor on metal surface [25]. Process of chemisorption includes transferring the charge from the inhibitor molecule into the metal surface. The significant negative entropy values

of activation in the absence and presence of the inhibitor imply that during the rate determining step, the activated complex formed is due to association instead of dissociation [**26**] which leads to reduced randomness between reactants and the activated complex [**27**].

Thermodynamic study: The adsorption isotherms such as Langmuir, Temkin, Frumkin and Flory-Huggins provide a clear image of the adsorption system. The surface coverage θ acquired by the potentiodynamic polarization were adapted to the aforementioned isotherms. The best fit is Langmuir model if the linear regression coefficient (R^2) and slopes are close to 1. The equation 12 provides the adsorption isotherm of Langmuir's for monolayer chemisorption [**28**].

$$\frac{Cinh}{\theta} = \frac{1}{K} + Cinh \qquad (12)$$

Where K represents the equilibrium constant, C_{inh} is concentration of the inhibitor and θ is surface coverage. Figure 9 shows the plot of Cinh/θ against C_{inh} . It gives a straight line with intercept 1/k. Furthermore, equation 14 is used to calculate the standard free energy change $\Delta G°_{ads}$.

$$K = \frac{1}{55.5}\exp\left(\frac{\Delta G° ads}{RT}\right) \qquad (13)$$

Where K is the constant, R is gas constant and T is the temperature and 55.5 is the concentration of water in mol dm^{3-1} [**29**]. A graph of $\Delta G°ads$ versus T is shown in figure 10. The standard enthalpy of adsorption ($\Delta H°ads$) and standard entropy of adsorption ($\Delta S°ads$) have been calculated from the slope and intercept of the straight line respectively and are listed in the table 5. The adsorption process spontaneity and stability of the adsorbed layer on the alloy were guaranteed by the negative values of $\Delta G°ads$. Generally $\Delta G°ads$ are approximately -20 $kJmol^{-1}$ or smaller, then it is physiosorption and if the values are more negative than -40 $kJmol^{-1}$ then it is chemisorption [**30**]. In the present case, $\Delta G°ads$ values are above -40 $kJmol^{-1}$ indicating that adsorption of NPOP on the 6063Al alloy surface may be completely due to chemisorption phenomenon. Also, positive value of $\Delta H°ads$ is attributable to chemisorption. The negative values of $\Delta S°ads$ indicate that the decline in disordering occurs when reactant becomes adsorbed.

Table 5. Thermodynamic parameters for the adsorption of NPOP on 6063 Al alloy surface in 0.5M HCl at different temperatures.

Temp K	$-\Delta G^0_{ads}$ (kJ/mol)	ΔS^0_{ads} (kJ/mol/K)	ΔH^0_{ads} (kJ/mol)
303	37.57		
313	38.44	-107.3	15.85
323	40.49		
333	42.17		

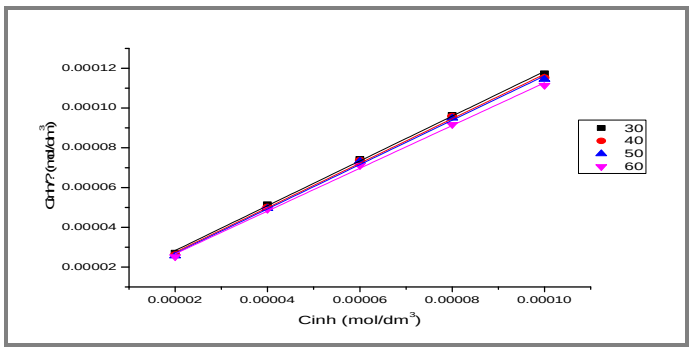

Figure 9. Langmuir adsorption isotherms for the adsorption of NPOP on 6063 Al alloy in 0.5M HCl at different temperatures.

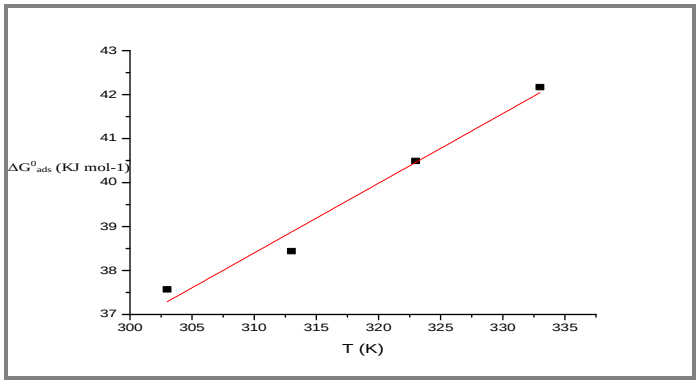

Figure 10. Plot of ΔG^0_{ads} versus T for the adsorption of NPOP on 6063 Al alloy in 0.5M HCl.

Surface analysis: Surface morphology of corroded and un-corroded alloy coupons was examined by SEM. Before immersion, the abrading scratches and pores can be clearly seen from the surface micrograph (Figure 11a). The surface of 6063Al alloy is drastically corroded with a slender morphology in the uninhibited solution (Figure 11b, 11c) shows the aggressive impact of HCl is heavily mitigated and pores are sealed by inhibitor, owing to oxide layer formation.

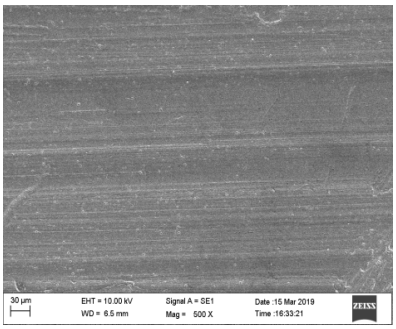

Figure 11a.
6063Al alloy surface

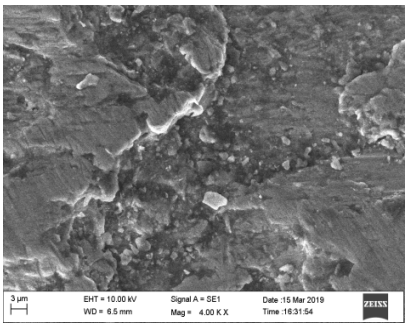

Figure 11b.
6063Al alloy + 0.5M HCl

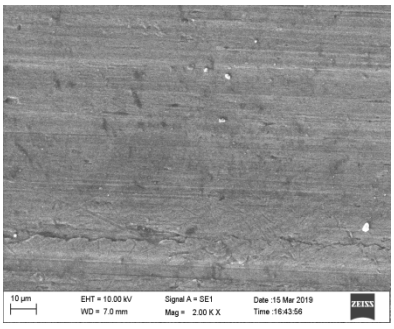

Figure 11c.
6063Al alloy+0.5MHCl + NPOP

Computational analysis

Quantum Chemical study: Quantum calculations of inhibitor molecules were performed to explore the adsorption and inhibition mechanism. The full geometry optimized structure is shown in figure 12. The frontier molecular orbital density distribution (HOMO and LUMO) of NPOP is shown in figure 13 and 14. The parameters, which directly affect the electronic interaction of the inhibitor with the metal are the frontier molecular orbital energies(E_{HOMO}, E_{LUMO}), E_{LUMO}- E_{HOMO}(ΔE), dipole moment (μ), global hardness (η) , softness (σ) electronegativity (χ) and mulliken charges [31]. All of these parameters support the search for an appropriate connection between molecular structure and inhibition effectiveness. Quantum chemical parameters computed for NPOP are listed in the table 6. The higher E_{HOMO} value indicates higher tendency of an inhibitor to donate lone pair of electrons to the vacant orbitals of the metal. E_{HOMO} facilitates an increased inclination for electron donations to the appropriate acceptor molecules with vacant orbitals by the inhibitor molecules. Lower E_{LUMO} value suggests that the inhibitor is a better acceptor of electrons from the occupied orbitals of the metal which shows good inhibition efficacy. Moreover, relative high organic molecular reactivity is associated with lower ΔE(HOMO and LUMO energy gap). Lower ΔE will trigger greater inhibition effectiveness because the energy to remove an electron from the last occupied orbital will be small. The greater value of μ favours the aggregation of the inhibitor in the surface layer [32]. NPOP with μ value of 4.0924D displays improved adsorption. Global hardness (η) and softness (σ) are the

characteristics for measuring the molecular stability and reactivity. Soft molecules are more reactive than hard ones because they readily provide electrons to acceptors. The lower the χ, the higher the molecule's likelihood of electron transfer and vice versa [**33**]. The Mulliken charges of NPOP molecule are shown in table 7. The highest negative charge is resided in oxygen atoms. There is an accord by several authors that the more negatively charged heteroatom is, the more is its ability to absorb on the metal surface [**34**]. The structural orientation and size of the inhibitor molecules play an important role in the embodiment of the adsorption steps, and compounds with benzene rings can be flatly oriented over the metal substratum due to the strong compatibility between the π-electrons of the rings and the metal surface.

Table 6. Quantum chemical parameters for NPOP

E_{HOMO}	E_{LUMO}	$\Delta E=E_{HOMO}-E_{LUMO}$	μ	$\eta=\frac{E_{HOMO}-E_{LUMO}}{2}$	$\sigma=1/\eta$	$\chi=-\frac{(E_{HOMO}+E_{LUMO})}{2}$
-0.3299 eV	-0.0281 eV	0.3018 eV	4.0924D	0.1509Ev	6.629Ev	0.179 eV

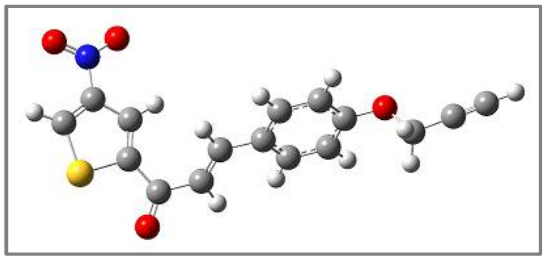

Figure 12. Optimised structure of NPOP.

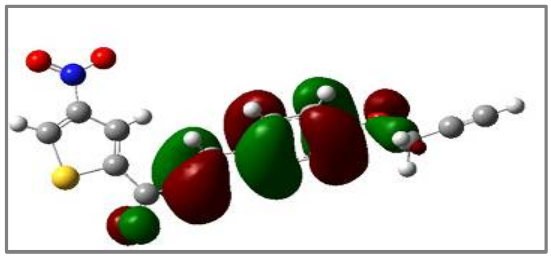

Figure 13. Structure for distribution of HOMO energy.

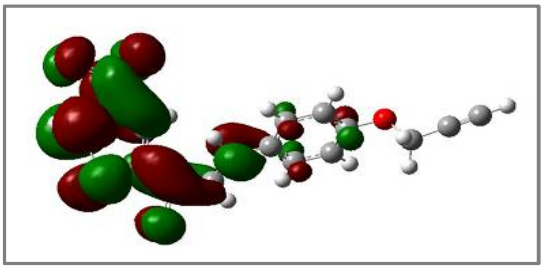

Figure 14. Structure for distribution of LUMO energy.

Table 7. Mulliken atomic charges for NPOP

1	C	-0.559031	12	O	-0.555858	23	H	0.265570
2	C	-0.125770	13	C	-0.287416	24	C	0.298628
3	C	0.363500	14	C	-0.175096	25	H	0.275427
4	C	-0.588957	15	H	0.282331	26	H	0.269783
5	S	0.773584	16	H	0.241525	27	O	-0.639983
6	H	0.318834	17	C	-0.090652	28	C	-0.051890
7	H	0.345324	18	C	-0.211023	29	H	0.252626
8	N	0.047598	19	C	-0.231689	30	H	0.250188
9	O	-0.319608	20	C	-0.243982	31	C	-0.076775
10	O	-0.336932	21	H	0.255985	32	C	-0.406864
11	C	0.555199	22	C	-0.239518	33	H	0.344942

Inhibition Mechanism: With regard to the inhibition process, the adsorption of the inhibitor on a metal/solution interface is generally assumed to be the first step in the inhibitor operating mechanism in aggressive acid media. NPOP molecule may be protonated, which might adsorb onto metallic

surface via the negatively charged acid anions (Cl^-). From it is evident that these compounds can be adsorbed on the metal surface through the lone pair electrons of nitrogen, oxygen atoms or delocalized π-electrons from heterocyclic ring. The inhibitory effect of NPOP can be described in this work by means of the molecular framework with accessible lone pairs of on N, S, O atoms and interactions with unshared π electrons of aluminium atoms. Single pair of nitrogen, sulphur and oxygen, electrons is easily accessible for sharing with metal atoms to form an indigenous covalent bond. The adsorbed inhibitor will thus cover the metal surface and defend it against corrosion.

Adsorption could lead from one or more of three relationships, viz. electrostatic attraction between charged molecules and charged metal, coordination of the unshared pairs of electron on the molecule to the metal atom and participation of π electrons of the inhibitor molecule in coordination system [**35**]. It is suggested that the metal surface is protected as a result of the creation of a co-ordinate bond between the inhibitor molecule and the metal. SEM picture also confirms the formation of protective film on the metal surface.

CONCLUSION

NPOP has been found to be an effective 6063Al alloy corrosion inhibitor at 0.5M HCl, the conclusions drawn are:

1. Studies of polarisation have shown that rising inhibitor concentration efficiently improves 6063 Al alloy corrosion resistance.
2. Increased inhibitor concentration and temperature has a beneficial impact on the efficacy of inhibition.
3. Mode of adsorption identified was Langmuir isotherm.
4. By regulating metal dissolution and hydrogen release, inhibitor functions as a prospective compound and thus acts as a blended inhibitor.
5. Activation energy values and thermodynamic presets favour chemical adsorption.
6. SEM has disclosed the development of protective film on the metal surface in terms of morphology, topography and rough nature of the metal surface.
7. Quantum chemical approach is adequately sufficient to predict the structure and molecule suitability to be an inhibitor.

REFERENCES

[1]. G. M. Scamans, N. Birbilis, R. G .Buchheit, Corrosion of Aluminium and its alloys, *Shreir's Corrosion*, **2010**, 3(1), 1974-2010.
[2]. N. L. Sukiman, X. Zhou, N. Birbilis, A. E. Hughes, J. M. C. Mol, S. J. Garcia, X. Zhou, G. E. Thompson, Durability and Corrosion of Aluminum and its Alloys: Overview, Property Space, Techniques and Developments, *Intech, Croatia, Europe*, **2011**, 49–97, 10.5772/53752.
[3]. W. A. Badawy, F. M. Al-Kharafi, A. S. El-Azab, Electrichemical behaviour and corrosion inhibition of Al, Al-6061 and Al-Cu in neutral aqueous solutions, *Corros. Sci.*, **1999**, 41(4), 709–727. https://doi.org/10.1016/S0010-938X(98)00145-0
[4]. F. Bentiss, M. Traisnal, M. Lagrenee, Inhibitor effects of triazole derivatives on corrosion of mild steel in acidic media, *Br. Corros, J.*, **2000**, 35(4), 315-320. https://doi.org/10.1179/000705900101501326
[5]. K. Raviprabha, S. B. Ramesh, Inhibition effects of Ethyl-2-Amino-4-Methyl-1,3-Thiazole-5-Carboxylate on corrosion of AA6061 alloy in hydrochloric acid media, *J. Fail. Anal. and Preven*, **2019**, 19(5), 1464-1474. DOI 10.1007/s11668-019-00744-5
[6]. F. Hunkeler, H. Bohni, Mechanism of pit growth on aluminium under open circuit conditions.Corrosion, **1984**, 40(10), 534-540. https://doi.org/10.5006/1.3593889
[7]. S. M. Abd El Haleem, S. Abd El Wanees, E. E. Abd El Aal, A. Farouk, Factors affecting the corrosion behaviour of aluminium in acid solutions. I. Nitrogen and/or sulphur containing

organic compounds as corrosion inhibitors for Al in HCl solutions. *Corros. Sci.*, **2013**, 68, 1-13. https://doi.org/10.1016/j.corsci.2012.03.021

[8]. F. Bentiss, M. Lebrini, M. Lagrenee,Thermodynamic characterization of metal dissolution and inhibitor absorption processes in mild steel /2,5-bis(n-thienyl)-1,3,4-thiadiazoles/hydrochloric acid system, Corros. Sci., **2005**, 47(12), 2915–293. https://doi.org/10.1016/j.corsci.2005.05.034

[9]. N. J. Baptiste, B. Kalluraya, Synthesis,characterization and antioxidant property of novel series of thiazole based chalcones carrying thiophene or furan derivatives. *Indian J.Heterocycl.Chem*., **2016**, 26(1-2), 69-74.

[10]. Asma, B. Kalluraya, N. Manju, Synthesis, characterization and antioxidant study of some novel chalcones carrying sydnonemoiety, *Der Pharma Chemica.,* **2017**, 9(10), 50-54.

[11]. N. J. Baptiste, B. Kalluraya, Synthesis,characterization and antioxidant evaluation of a novel series of chalcone derivatives bearing 2-hydroxy bearing moiety, *Der Pharma Chemica*., **2016**, 8(5), 167-172.

[12]. B. S. Holla, B. Kalluraya, K. R.Sridhar, On the synthesis of some 1-(5-Nitri-2-furyl)-3-aryl-2-propen-1-ones, *Curr.Sci.*, **1986**, 55(2),73-76.

[13]. B. S. Holla, B. Kalluraya, K. R. Sridhar, Synthesis of some 1-aryl-3-(5-Nitro-2-furyl)-2-propen-1-ones as potential antibacterial agents, Curr. Sci., **1987**, 56(12), 585-588.

[14]. S. Velrani, R. Mahalakshmi, Investigation of inhibition effect of naphthyl chalcones on mild steel corrosion in sulphuric acid medium, *Rasayan J. Chem.,* **2015**, 8(2),156-160.

[15]. A. S.Fouda, K. Shalabi, G. Y. Elewady, H. F. Merayyed, Chalcone derivatives as corrosion inhibitors for carbon steel in 1 M HCl solutions, *Int. J. Electrochem. Sci.*, **2014**, 9(12), 7038-7058.

[16]. R. Rosliza, H. B. Senin, W. B. WanNik, Electrochemical properties and corrosion inhibition of AA6061in tropical sea water, *Colloids Surf.A.*, **2008**, 312(2-3),185-189. https://doi.org/10.1016/j.colsurfa.2007.06.061

[17]. E. S. Ferreira, C. Giacomelli, F. C. Giacomelli, A. Spinelli,Evluation of the inhibitor effect of L-ascorbic acid on the corrosion of mild steel, *Mater. Chem. Phys.,* **2004**, 83(1), 129-134 https://doi.org/10.1016/j.matchemphys.2003.09.020

[18]. W. Li, Q. He, C. Pei, B. Hou, Experimental and theoretical investigation of the adsorption behaviour of new triazoles derivatives as inhibitors of mild steel corrosion in acid media, Electrochim.Acta., **2007**, 52(22), 6386-6394. https://doi.org/10.1016/j.electacta.2007.04.077

[19]. V. O. Njoku, E. E. Oguzie, C. Obi, A. A. Ayuk, *Baphianitida* Leaves extract as a green corrosion inhibitor for the corrosion of mild steel in acidic media, Adv.Chem., **2014**, 1-10. http://dx.doi.org/10.1155/2014/808456

[20]. G. M. Pinto, J. Nayak, A. N. Shetty, Corrosion inhibition of 6061Al-15 vol.pct.SiC(p) composite and its base alloy in a mixture of sulphuric acid and hydrochloric acid by 4-(N,N-dimethyl amino) benzaldehyde thiosemicarbazone. *Mater. Chemand Phys.*, **2011**, 125(3), 628-640. https://doi.org/10.1016/j.matchemphys.2010.10.006

[21]. M. A. Migahed, Electrochemical investigation of the corrosion behaviour of mild steel in 2 M HCl solution in presence of 1-dodecyl-4-methoxy pyridinium bromide, *Mater. Chem and Phy,* **2005**, 93(1), 48-53. https://doi.org/10.1016/j.matchemphys.2005.02.003

[22]. A. K. Singh, M. A. Quraishi, Effect of cefazolin on the corrosion of mild steel in HCl solution, *Corr. Sci.*, **2010**, 52(1), 152-160. https://doi.org/10.1016/j.corsci.2009.08.050

[23]. E. Machnikova, K. H. Whitmire, N. Hackerman, Corrosion inhibition of carbon steel in hydrochloric acid by furan derivatives, *Electrochim. Acta*, **2008**, 53(20), 6024-6032. https://doi.org/10.1016/j.electacta.2008.03.021

[24]. M. Scgorr, J. Yahalom, The significance of the energy of activation for the dissolution reaction of metal in acids, *Corr. Sci.,* **1972**, 12(11), 867-868. https://doi.org/10.1016/S0010-938X(72)80015-5

[25]. A. Popova, M. Christov, S. Raicheva, E. Sokolova, Adsorption and inhibitive properties of benzimidazole derivatives in acid mild steel corrosion, *Corr.Sci.*, **2004**, 46(6), 1333-1350. https://doi.org/10.1016/j.corsci.2003.09.025

[26]. A. Hamdy, N. S. El-Gendy, Thermodynamic, adsorption and electrochemical studies for corrosion inhibition of carbon steel by henna extract in acid medium, *Egypt J Pet.*, **2013**, 22(1), 17-25. http://dx.doi.org/10.1016/j.ejpe.2012.06.002
[27]. N. Soltani, M. Behpour, S. M. Ghoreishi, H. Naeimi, Corrosion inhibition of mild steel in hydrochloric acid solution by some double Schiff bases, *Corr.Sci*., **2010**, 52(4), 1351-1361. doi:10.1016/j.corsci.2009.11.045
[28]. Z. Tao, S. Zhang, W. Li, B. Hou, Corrosion inhibition of mild steel In acidic solution by some oxo-triazole derivatives, *Corr. Sci.,* **2009**, 51(11), 2588-2595. doi:10.1016/j.corsci.2009.06.042
[29]. A. M. Fekry, M. A. Ameer, Corrosion inhibition of mild steel in acidic media using newly synthesized heterocyclic organic molecule, *Int. J. Hydrogen Energy*, **2010**, 35(14), 7641-7651. doi:10.1016/j.ijhydene.2010.04.111
[30]. S. P. Fakrudeen, H. C. A. Murthy, V. B. Raju, Corrosion inhibition of AA6061and AA6063 alloy in hydrochloric acid media by Schiff base compounds, *J. Chil. Chem. Soc.*, **2012**, 57(4), 1364-1370.
[31]. J. Bhawsar, P. K. Jain, P. Jain, Experimental and computational studies of *Nicotiana tabacum* leaves extract as green corrosion inhibitor for mild steel in acidic medium, *Alexandria Eng. J.*, **2015**, 54(3),769–77. http://dx.doi.org/10.1016/j.aej.2015.03.022
[32]. L. O. Olasunkanmi, I. B. Obot, M. M. Kabanda, E. E. Ebenso, Some quinoxaline -6-yl derivatives as corrosion inhibitors for mild steel in hydrochloric acid: Experimental and theoretical studies, *J. Phys. Chem. C.,* **2015**, 119(28), 16004-16019. DOI: 10.1021/acs.jpcc.5b03285
[33]. L. O. Olasunkanmi, M. F. Sebona, E. E. Ebenso, Influence of 6-phenyl-3 (2H)-pyridazinone and 3-chloro-6-phenylpyrazine on mild steel corrosion in 0.5 M HCl medium: Experimental and Theoretical Studies, *J. Mol. Struct.*, **2017**, 1149, 549-559. doi: 10.1016/j.molstruc.2017.08.018.
[34]. S. K. Saha, M. Murmu, P. Banerjee, Evaluating electronic structure of quinazolinone and pyrimidinone molecules for its corrosion inhibition effectiveness on target specific mild steel in the acidic medium: A combinent DFT and MD simulation study, *J. Mol. Liq.*, **2016**, 224(B), 629-638. doi:10.1016/j.molliq.2016.09.110
[35]. S. Martinez, I. Stern, Thermodynamic characterization of metal dissolution and inhibitor adsorption processes in the low carbon steel/mimosa tannin/sulphuric acid system, *Appl. Surf. Sci*., **2002**, 199(1-4), 83-89. https://doi.org/10.1016/S0169-4332(02)00546-9